FINITE ELEMENT NUMERICAL ANALYSIS OF THE BEARING CAPACITY OF HYBRID FIBER REINFORCED CONCRETE PIPES

Federico A. González

Viviana C. Rougier

gonzalezf@frcu.utn.edu.com.ar

vrougier@frcu.utn.edu.com.ar

UTN - FRCU - FRCon

Ingeniero Pereira 676, 3260, Concepción del Uruguay, Entre Ríos, Argentina.

Mario R. Escalante

mescalante@frcu.utn.com.ar

UTN - FRCU

Concepción del Uruguay, Entre Ríos, Argentina.

Abstract. *Reinforced concrete with two or more types of fibers, rationally combined (hybrid fiber reinforced concrete, HFRC) may offer enhanced properties, especially in terms of ductility and crack control. The use of these concretes in drainage pipes, either partially or totally substituting steel meshes and bars of traditional reinforcement, might have a favorable impact on the optimization of the product in the precast industry from both technical and economic point of view. The HFRC can be prepared and placed into molds in a similar way as for plain concrete, where the fibers are added to the mix just like any other aggregate. In this paper, as part of an initial stage of an on going research, the mechanical behaviour of hybrid reinforced concrete pipes (steel and polypropylene) is numerically assessed by simulation of the three-edge bearing test (TEBT). The HFRC is modeled as a homogeneous material with equivalent properties (macro model), in which the characteristic parameters of the material, used in the simulation, are obtained through an experimental study. The problem is solved by a nonlinear finite element code in which a coupled damage and plasticity constitutive model is used.Finally, the results are compared with experimental data obtained by another author.*

Keywords: *numerical analysis, bearing capacity, hybrid fiber reinforced concrete, concrete pipes.*

1 INTRODUCTION

Concrete is a structural material widely used throughout the world. It has been the subject of continuous research in the construction industry. In part, this occurs due to the fact that this composite presents certain limitations, such as low capacity of deformation and rapid propagation of cracks when submitted to tensile stresses

The addition of steel fibers to concrete (SFRC) has been a technological success in improving the tensile properties of concrete. This concept was extended to the production of hybrid fiber reinforced concrete (HFRC).

HFRC is a mix of concrete matrix and fibers with different material and geometric properties that results in synergistic and superior performance compared to the use of only one type of fibers [Ibrahim et al., 2016], i.e. two or more than two types of fibers contributing towards the mechanical properties both individually and as a group [Almusallan et al., 2016].

Compared to the plain concrete (PC), the increase in the toughness of the HFRC is mainly due to the fiber bridging and good bond behavior. The major role played by the fibers in the composite occurs in the post cracking zone wherein redistribution of the load between the matrix and the fibers occurs [Banthia et al., 2003; Banthia et al., 2014]. There is a wide application of HFRC in precast concrete elements with reduced sections, improved impact resistance and crack control [Banthia, 2012].

In cast concrete pipes, the manufacturing of the steel reinforcing cage from conventional steel rebar requires special bending, welding, and placement machinery, which is costly and time-consuming [Mohamed, 2015]. An efficient alternative used when replacing steel rebar reinforcement is the addition of randomly distributed fibers forming what has been termed fibre reinforced concrete (FRC) [Alberti et al, 2016]. The fibers, can be added into the mixer of any concrete batch plant, similar to the other mixture ingredients, without significant process modification. The FRC can be produced and cast in pipe molds like ordinary plain concrete (Figure 1). Therefore, FRC pipes can be an economical alternative to the conventionally reinforced concrete pipes [Banthia, 2012].

Steel fibres can greatly improve the tensile strength and the flexural strength of concrete, when used for concrete pipes precast, due to their ability to absorb energy [Beglarigale et al., 2015] and control cracks. However, they may suffer durability problems in aggressive environments [Alberti et al., 2016]. The corrosion of steel fibers can be detrimental and lead to rapid deterioration of concrete structures [Soylev and Ozturan, 2014]. The polymer macrofibers do not suffer from electrolytic corrosion, which, unlike steel fibers, translates into a gain in potential durability. In addition, they do not greatly affect the workability of the material, since they are more flexible [Figueiredo et al., 2012]. However, steel fibers provide superior mechanical properties, especially tensile strength and toughness, due to their high modulus of elasticity.

In terms of the manufacturing of FRC pipes, there are codes that regulate their use [EN 1916: 2002; UNE-EN 1916: 2008; ABNT-NBR 8890: 2007]. However, among the numerous studies conducted in the literature references, limited studies have been performed on the effect of a combination of fibers in concrete pipes [Park et al., 2015].

The principal aim of this paper, as part of an initial stage of an on going research, is to obtain information about the bearing capacity of hybrid reinforced concrete pipes (steel and polypropylene) through the simulation of the TEBT using the mechanical properties of the

Figure 1: Molding and vibrating process. Demolding

HFRC obtained from experimental tests. The model is implemented in Abaqus [ABAQUS] and the results are compared with those obtained by another author [Mohamed, 2015]

2 MODELLING THE THREE EDGE BEARING TEST

The TEBT is the standard test that is commonly used for evaluating the bearing capacity of concrete pipes in the precast concrete pipes industry. In this test, the load is applied as a line load along the crown of the pipe, while the pipe is supported by two closely spaced bearing strips along the invert [Mohamed et al., 2016]. ASTM C497 [ASTM C497] specifies the test procedure and requirements for the testing apparatus, upper and lower bearings, spacing between lower bearings, and the loading rate, Figure 2.

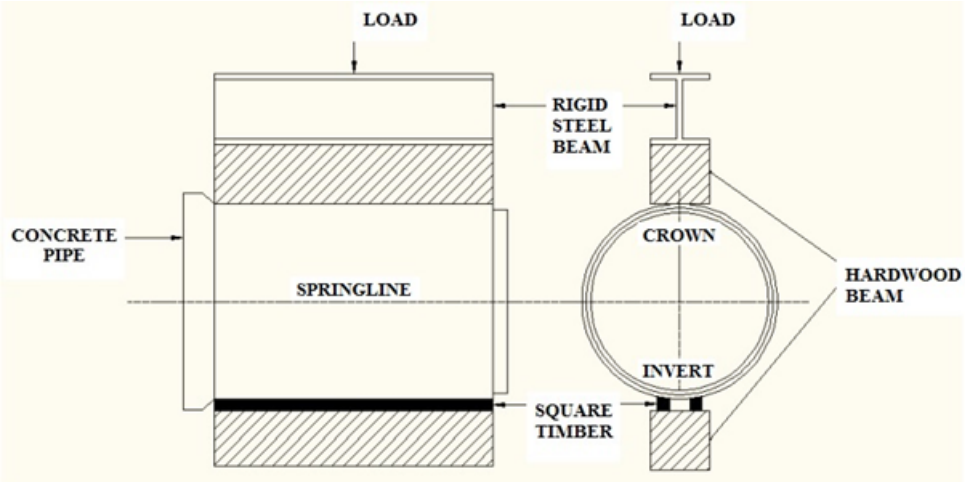

Figure 2: Three-edge bearing test

A 2D plane strain model in ABAQUS was used for simulating the TEBT. The upper loading support, two lower supporting strips and the concrete pipe were modeled. The supports are 50 mm wide and 50 mm high and the spacing between them is 50 mm and were modeled as rigid elastic. Displacement-controlled method was accomplished by applying a 20 mm downward displacement at the upper bearing strip. For the pipe, 3-node linear triangular elements in plane strain state were used.

2.1 Concrete damage plasticity model

Two concrete constitutive models are available in ABAQUS software. These are the concrete smeared cracking model (CSCM) and the concrete damaged plasticity model (CDPM). As the CSCM is known to have difficulty converging after steel yielding [Chen and Graybeal, 2012], CDPM was used in this paper.

CDPM is a continuum, plasticity-based, and damage model for concrete. It assumes that the main two failure mechanisms are tensile cracking and compressive crushing of the concrete material. The model mainly includes four major components, namely, the damage evolution, yield criterion, hardening/softening law and flow rule.

Damage. Traditionally, in order to reflect the concrete nonlinearity and irreversible deformation, the total strain ϵ can be decomposed into two parts according to the classic elasto-plasticity theory,

$$\epsilon = \epsilon^{pl} + \epsilon^{el} \tag{1}$$

where ϵ^{el} and ϵ^{pl} are the elastic and plastic strains, respectively. Numerous test results have evidenced that the concrete nonlinearity can be attributed to damage or plasticity individually, or stem from a combination of both, while the degradation of unloading stiffness is mainly associated with the damage evolution. Hence, during the numerical simulation, it is desirable to isolate the effect of damage from that of plasticity reasonably [Chi and Yu, 2014].

CDPM offers a general capability for modelling progressive material damage, in which a scalar damage variable d, $0 \leq d \leq 1$,is introduce;

$$\sigma_{ij} = (1-d){D_{ijkl}}^{el}(\epsilon_{ij} - {\epsilon_{ij}}^{pl}) \tag{2}$$

where σ_{ij} is the function of stress state, ${D_{ijkl}}^{el}$ is the initial elasticity matrix, ϵ_{ij} is the strain tensor and ${\epsilon_{ij}}^{pl}$ is the plastic strain tensor. The stiffness degradation is defined by degradation variable d_c in compression zone and variable d_t in a tension zone.

In this model the tensile and compression response is characterized though differentiated uniaxial stress-strain curves, as show in Figure 3, where σ_{c0} is the ultimate compression stress, ϵ_c^{in} is the crushing strain, $\epsilon_{oc}^{el} = \sigma_c/E_0$, σ_{t0} is the failure tensile stress, ϵ_t^{ck} is the cracking strain and $\epsilon_{ot}^{el} = \sigma_t/E_0$.

Plastic flow. The concrete damaged plasticity model assumes nonassociated potential plastic flow. The flow potential G used for this model is the Drucker-Prager hyperbolic function:

$$G = \sqrt{(\epsilon.\sigma_{t0}.tan\psi)^2 + q^2} - p.tan\psi \tag{3}$$

where:

p = hydrostatic pressure stress tensor.

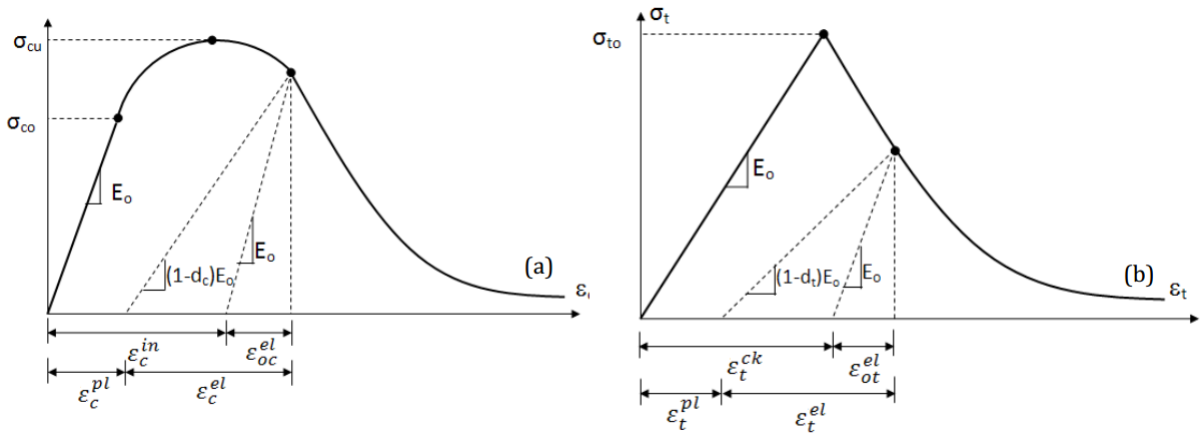

Figure 3: Compression curve $\sigma_c - \epsilon$ (a); Tensile curve $\sigma_t - \epsilon$ (b)

q = equivalent Mises stress tensor.

ψ = dilation angle measured in the tensile meridian.

σ_{to} = is the uniaxial tensile stress at failure.

ϵ = is a parameter, referred to as the eccentricity, which defines the rate at which the function approaches the asymptote (the flow potential tends to a straight line as the eccentricity tends to zero).

Yield function The model makes use of the yield function of Lubliner et. al. (1989) [Lubliner et al., 1989], with the modifications proposed by Lee and Fenves (1998) [Lee and Fenves, 1998] to account for different evolution of strength under tension and compression. In terms of effective stresses, the yield function takes the form:

$$F = \frac{1}{1-\alpha}(q - 3\alpha p + \beta(\epsilon^{pl})(\sigma_{max}) - \gamma(-\sigma_{max}) - (\sigma_c(\epsilon^{pl})) = 0 \tag{4}$$

with:

$$\alpha = \frac{\frac{\sigma_{b0}}{\sigma_{c0}} - 1}{\frac{2\sigma_{b0}}{\sigma_{c0}} - 1}; 0 < \alpha < 0.5 \tag{5}$$

$$\beta = \frac{\sigma_c(\epsilon_c^{pl})}{\sigma_t(\epsilon_t^{pl})}(1-\alpha)(1+\alpha) \tag{6}$$

$$\gamma = \frac{3(1-K_c)}{2(K_c-1)} \tag{7}$$

where ϵ^{pl} is the hardening(softening)variable, σ_{max} is the maximum principal effective stress, σ_{b0}/σ_{c0} is the ratio of initial equibiaxial compressive yield stress to initial uniaxial compressive yield stress, K_c is the ratio of the second stress invariant on the tensile meridian, σ_t is the effective tensile cohesion stress, and σ_c is the effective compressive cohesion stress.

Hardening/softening. The hardening/softening law features the shape and location of the loading surface, as well as its evolution after initial yielding, wherein the hardening law describes the pre-peak behaviour as the elastic region terminates and softening law defines to the post-peak behaviour during plastic flow [Chi et al., 2014].

In ABAQUS, an isotropic hardening is assumed and the evolution law is driven by the equivalent plastic strain, as indicated in Eq. 4.

2.2 Material characterization tests

The experimental study consisted in performing compression tests and three-point bending test (TPBT) on specimens of HFRC and SFRC. The TPBT can be considered as the basic procedure for evaluating FRC. [Figueiredo et al., 2011].

The aim of the tests was to obtain: a) compression strength the material (SFRC and HFRC), to be used as a parameter in the model adopted for the compression behaviour curve (see section 2.3); b) the tensile behaviour curve (see section 2.3).

The experimental tests were carried out at the Civil Engineering Laboratory of UTN University of Concordia, Argentina. As mentioned above, the HFRC specimens were obtained by mixing two types of fibers (Figure 4): Steel fibers (S) labeled Wirand FF3; and Polypropylene fibers (P) labeled Macronita. Their geometric and mechanical properties are summarizes in Table 1.

Figure 4: Steel (left) and Polypropylene (right) fibers

Table 1: Relevant properties of fibers

Fibers		Diameter [mm]	Length [mm]	Tensile strength [MPa]	Elastic Modulus [GPa]
Steel (S)	WIRAND FF3	1	50	$\geq$ 1200	210
Polypropylene (P)	MACRONITA	0.60	50	400-500	3.5-3.9

P fibers present an aspect ratio (AR) length/diameter (equal to 83) higher than the S ones (AR = 50), being the latter characterized by significantly higher tensile strength and elastic modulus.

Two mixtures were prepared, one with a dosage of P and S fibers of 2,8 kg/m^3 and 20 kg/m^3 respectively, and another mix having only S fiber with a dosage of 25 kg/m^3. In addition, a PC mixture volume was extracted as a reference.

The concrete mixtures composition is reported in Table 2.

Table 2: Concrete mixes composition

Cement	$[kg/m^3]$	370
Fine sand	$[kg/m^3]$	605
Coarse Aggregate		
Max. size = 19mm	$[kg/m^3]$	646
Max. size = 12.5mm	$[kg/m^3]$	646
Ratio w/c	$[l/m^3]$	0.45
Super plasticer	$[l/m^3]$	3
Compressive strength	$[MPa]$	30

A total number of 6 prismatic specimens were prepared for the TPBT (2 PC; 2 HFRC; 2 SFRC). Moreover, 12 cylindrical specimens (300 mm in height and 150 mm in diameter) were realized for the uniaxial compressive tests (6 PC; 3 HFRC; 3 SFRC). All specimens were tested at 28 days of curing [IRAM 1534/04].

The compressive tests were performed in displacement control according to IRAM 1546/92 [IRAM 1546/92] provisions. Table 3 shows the results of the tests.

The TPBT tests were carried out as recommended by RILEM [RILEM TC 162-TDF., 2002]. The table 4 show the average values for flexural tensile strength and Residual flexural tensile strengths $f_{R,i}$ for crack opening displacement($CMOD_1$,$CMOD_2$,$CMOD_3$ and $CMOD_4$).

Table 3: Results obtained by the tests

Group	Specimens	Compression strength
		Average (MPa)
Mix 1	Plain Concrete	37.87
Mix 1	HFRC	38.15
Mix 2	Plain concrete	39.67
Mix 2	SFRC	44.38

2.3 Material behaviour on compressive and tensile

As mentioned previously, CDPM adopted the differentiated uniaxial stress-strain curves. These are obtained as explained below:

Table 4: TPBT results

Specimens	Flexural Tensile Strength Av. (MPa)	$CMOD_1$ $f_{R,1}$(MPa)	$CMOD_2$ $f_{R,2}$(MPa)	$CMOD_3$ $f_{R,3}$(MPa)	$CMOD_4$ $f_{R,4}$(MPa)
HFRC	4.10	1.79	1.63	1.42	1.17
SFRC	3.84	2.90	3.16	2.99	2.75

Compressive Behaviour. In the next stages of the research, the uniaxial compression curve will be obtained from experimental tests. In this paper, was adopted the model proposed by Barros and Figueiras [Barros and Figueiras, 1999], because it same was use in the paper of Mohammed [Mohamed, 2015] with which the results obtained are compared. The expression is based on the following relationships:

$$\sigma_c = \frac{\frac{\epsilon_c}{\epsilon_{c1}}}{(1-p-q)+q(\frac{\epsilon_c}{\epsilon_{c1}})+p(\frac{\epsilon_c}{\epsilon_{c1}})^{\frac{1-q}{p}}} \tag{8}$$

with:

$$q = 1 + p - \frac{E_{pf}}{E_c}, \tag{9}$$

$p+q \in]0,1[, \frac{1-q}{p} > 0$

$$E_{pf} = \frac{f_{cf}}{\epsilon_{pf}} \; ; E_c = 21.500(\frac{f_{cf}}{10})^{(1/3)} \tag{10}$$

Where f_{cf} is the compressive strength, obtained by experimental tests, as mentioned in section 2.2.

For hooked-end fibres ($l_f = 30mm, d_f = 0.50mm, l_f/d_f = 60$):

$$\epsilon_{pf} = \epsilon_{co} + 0.0002Wf \tag{11}$$

$$p = 1 - 0.919e^{-0.394W_f} \tag{12}$$

For hooked-end fibres ($l_f = 60mm, d_f = 0.8mm, l_f/d_f = 75$):

$$\epsilon_{pf} = \epsilon_{co} + 0.00026Wf \tag{13}$$

$$p = 1 - 0.722e^{-0.144W_f} \tag{14}$$

where: ϵ_{co} = strain at peak for plain concrete (0.0022 according to CEB-FIP Code 1999 [CEB-FIP, 1993]), ϵ_{pf} is the strain at peak stress, and W_f is the fibre weight percentage in the mixtures, 0.95 % and 1.04 % for HFRC and SFRC, respectively. Figure 5a shows the compression stress-strain curves used.

Tensile Behaviour. Although a direct tensile test is the most reliable method for determining the residual (post-cracking) properties of FRC, it is expensive. It requires specialized testing machines and can be time-consuming in its preparation[Amin, 2015]. For this reason, the tensile response was obtained by inverse analysis of data obtained from TPBT. Figure 5b shows the Tensile Stress-Crack width opening curves. These are the average curves of the specimens tested.

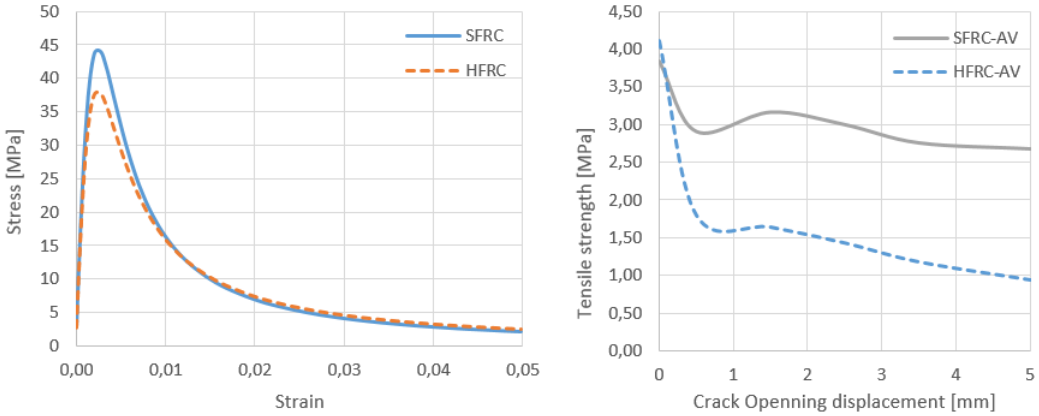

Figure 5: a) Compression stress curve $\sigma_c - \epsilon$; b) Tensile Stress - Crack Openning displacement

2.4 Numerical results

A pipe with 450mm of diameter and 82mm of wall thickness was modeled. Figure 6 show the Finite element mesh and model used.

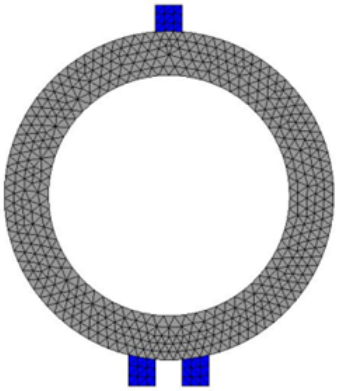

Figure 6: Finite element mesh

The values of the parameters (material properties) required by the CDPM are shown in Table 5. They are the ones recommended by Abaqus [ABAQUS] and have been used by other authors to model both steel [Mohamed, 2015; Ferrado et al., 2016] and synthetic [Abhaee, 2016] fiber reinforced concrete. As a first approximation, they have also been adopted for this paper.

The damage process was not activated in the simulation of this test, since damage process is more suitable for cases of brittle breaking behaviour such as plain concrete [Abhaee, 2016].

Two mixtures were studied, HFRC with 20 kg/m^3 and 2.8 kg/m^3 of S fibers and P fiber respectively, and SFRC with 25 kg/m^3 of S fibers.

Ultimate loads (D_{ult})were obtained using the model. Table 6 shows numerical results for hybrid fiber reinforced concrete pipe (HFRCP) and steel fiber reinforced concrete pipe (SFRCP)studied. Also, the experimental results obtained by another author [Mohamed, 2015] are shown. The pipe modeled in this work has the same thickness and diameter as the one used

Table 5: Parameters used in CDPM

Dilation Angle	36.51
Flow potential eccentricity	0.1
Viscosity parameter	0
σ_{b0}/σ_{c0}	1.16
K_c	0.67

by Mohamed [Mohamed, 2015]. However, the fiber is geometry and the dosage are not the same.

Table 6: Ultimate loads D_{ult}; obtained experimentally by Mohamed (SS4530, SL4530); obtained in this paper through simulation of the TEBT (HFRCP, SFRCP)

Designation	ϕ_{pipe} [mm]	Fibre Type	W_f $[Kg/m^3]$	h [mm]	f'_c [MPa]	D_{ult} [N/m/mm]	
SS4530	450	Steel fibers	30	82	42.5	256.7	EXP.-Mohamed
SL4530	450	Steel fibers	30	82	35.8	273.9	EXP.-Mohamed
HFRCP	450	Mix fibres	20/2.8	82	38.1	266	FEM.
SFRCP	450	Steel fibres	25	82	44.3	255	FEM.

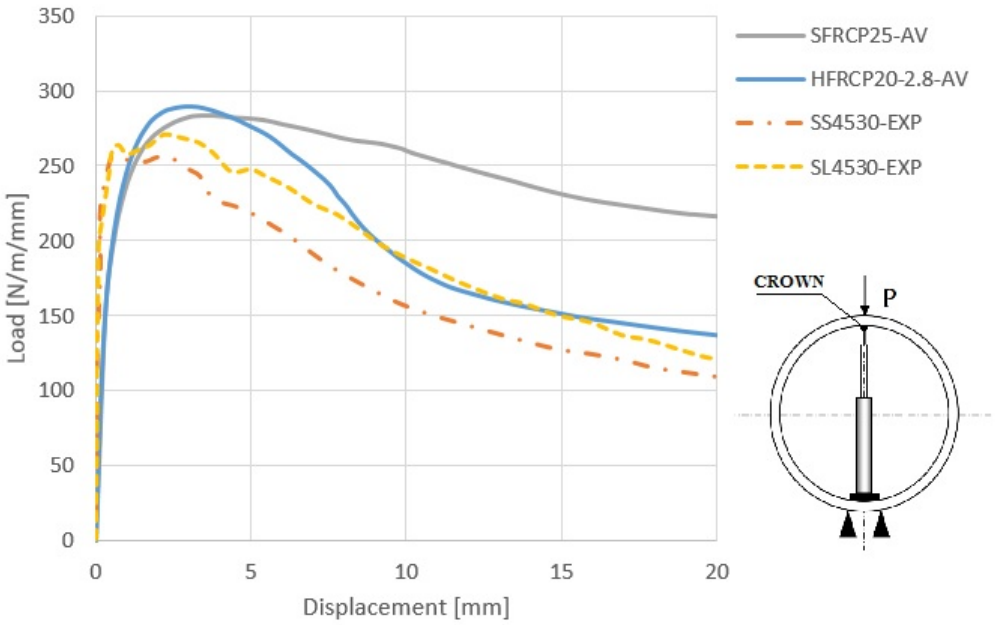

Figure 7: Load - Displacement at the crown

Figure 7 shows four Load-displacement curves at the point of the crown. SS4530-EXP and SL4530-EXP are experimental curves obtained by Mohamed [Mohamed, 2015] for 450mm di-

ameter pipes and $30Kg/m^3$ dosage of steel fibers and two different geometries; with short fibers (SS, Aspect ratio = 60) and long fibers (SL, Aspect ratio = 65) and concrete whose compressive strength average was 42.50 and 35.8 MPa respectively. FRCP25-AV and HFRCP20-2.8-AV are the average curves obtained by simulation tests with the mixes studied.

3 CONCLUDING REMARKS

The Three-edge bearing test was simulate for studing the bearing capacity of HFRC pipes. The characteristics of the material, such as compression strength and tensile behaviour, were obtained from experimental tests. A 2D model in plain strain state was adopted, in which the HFRC was modeled as homogeneous material was used.

From the results obtained, it could be said that the HFRC pipe reached a higher ultimate load than the SFRC pipe. It is observed that the SFRC pipe showed a greater ductility in the pospeak behaviour. In addition, the curve would be similar in shape, to the one obtained experimentally in the work of Mohamed. The HFRC pipe curve would show a pronounced descending arm in the pospeak behaviour.

It should be remarked that the next step, will be, on one hand, to perform a greater number of characterization tests to obtain more representative values to be used in the model and the other hand, to calibrate the model through experimental tests in HFRC pipes.

REFERENCES

ABAQUS. 6.13-EF. *Dassault Systems Simulia Corporation* Providence, RI, USA, 2014.

ABNT-NBR 8890:2007. Tubo de concreto, de seção circular, para águas pluviais e esgotos sanitários.

Abhaee S., 2016. Investigation of fiber-reinforced concrete crack width measurement by finite element method. *Master of science. University of Texas, Texas, United States.*

Alberti M., Enfedaque A., Gálvez J. C. and Agrawal V., 2016. Reliability of polyolefin fibre reinforced concrete beyond laboratory sizes and construction procedures. *Composite Structures*, Vol. 140, pp.506-524.

Almusallam T., Ibrahim S., Al-Salloum Y., Abadel A. and Abbas H., 2016. Analytical and experimental investigations on the fracture behavior of hybrid fiber reinforced. *Cement and Concrete Composites*, Vol. 74, pp.201-217.

Amin A., Foster S. and Muttoni A., 2015. Derivation of the $\sigma - w$ relationship for SFRC from prism bending tests. *Structural concrete*, pp.93-105.

ASTM C497-13,2013. Standard test methods for concrete pipe, manhole sections or tile. *American Society for Testing and Materials, ASTM International, West Conshohocken*.

Banthia N., Majdzadeh F., Wu J. and Bindiganavile V., 2012. Fiber synergy in Hybrid Fiber Reinforced Concrete (HyFRC) in flexure and direct shear. *Cement and Concrete Composites*.

Banthia N. and Majdzadeh F., Wu J., Bindiganavile V., 2014. Fiber synergy in hybrid fiber reinforced concrete (HyFRC) in flexure and direct shear. *Cement Concrete Composite*, Vol. 48, pp.91-97.

Banthia N. and Nandakumar N., 2003. Crack growth resistance of hybrid fiber reinforced composite. *Cement Concrete Composite*, Vol. 25, pp.3-9.

Barros J. and Figueiras J., 1999. Flexural behavior of SFRC: testing and modeling. *Journal Material Civil Engeneering*, Vol. 11, pp.331-339.

Beglarigale A. and Yazici H., 2015. Pull-out behavior of steel fiber embedded in flowable RPC and ordinary mortar. *Construction and Building Materials*, Vol. 75, pp.255-265.

Bencardino F., Rizzuti L.,Spadea G. and Swamy R., 2008. Stress-Strain behaviour of steel fiber reinforced concrete in compression. *Journal Material Civil Engeeniering*, Vol. 20, pp.255-263.

Chen L. and Graybeal B., 2012. Modeling Structural Performance of Ultrahigh Performance Concrete I-Girders. *Journal of bridge engineering*, Vol. 17, pp.754-764.

Chi Y., Xu L. and Yu H., 2014.Plasticity model for hybrid fiber-reinforced concrete under true triaxial compression. *Journal Engeneering Mechanical*, Vol. 140, pp.393-405.

Chi Y., Xu L. and Yu H., 2014. Constitutive modeling of steel-polypropylene hybrid fiber reinforced concrete using a non-associated plasticity and its numerical implementation. *Composite Structures*, Vol. 111, pp.497-509.

Chi Y., Xu L. and Zhang Y., 2014. Constitutive modeling of steel-polypropylene hybrid fiber reinforced concrete using a non-associated plasticity and its numerical implementation. *Journal Material Civil Engeneering*, Vol. 26, pp.211-218.

Comité euro-internacional du béton, 1993. CEB-FIP Model Code 1990: Design Code. *FIB-Fédération International du Béton.* No 213-214.

EN 1916:2002. Concrete pipes and fittings, unreinforced, steel fibre and reinforced.

Ferrado F., Escalante M. and Rougier V., 2016. Numerical simulation of the three edge bearing test of steel fiber reinforced concrete pipes. *Mecnica Computacional*, Vol. 34, pp.2329-2341.

Figueiredo A., de la Fuente A., Aguado A., Molins C. and Chama Neto P., 2011. Steel fibre reinforced concrete pipes. Part 1: technological analysis of the mechanical behaviour. *Revista RIEM*, Vol. 5, pp.1-11.

Figueiredo A., de la Fuente A., Aguado A. and Escariz R., 2012. Fibras plásticas como reforço de tubos de concreto. Parte 1: caracterização tecnológica. *Anais do 54 Congresso Brasileiro do Concreto*.

Ibrahim S., Almusallam T., Al-Salloum Y. and Abade A., 2016. Strain Rate Dependent Behavior and Modeling for Compression Response of Hybrid Fiber Reinforced Concrete. *Latin American journal. solids structures*, Vol. 13, pp.1695-1715.

IRAM 1534, 2004. Hormigón. Preparación y curado de probetas en laboratorio para ensayos de compresión y de tracción por compresión diametral. *Instituto Argentino de Normalización y Certificación*

IRAM 1546,1992. Hormigón de cemento pórtland. Método de ensayo de compresión. *Instituto Argentino de Normalización y Certificación*

Lee J. and Fenves G., 1998. Plastic damage model for cyclying loads of concrete structures. *Latin American journal. solids structures*, Vol. 124, pp.892-900.

Lubliner J., Oliver J. and Oller S., 1989. Plastic-damage model for concrete. *International Journal of solids and structures*, Vol. 25, pp.299-326.

Mohamed N.,2015 *Ph.D. thesis, The university of western Ontario*, Ontario, Canada.

Mohamed N. and Nehdi M., 2016. Rational finite element assisted design of precast steel fibre reinforced concrete pipes *Engeneering Structures*, Vol. 124, pp.196-206.

Park Y., Abolmaali A., Mohammadagha M. and Lee S., 2015. Structural performance of dry-cast rubberized concrete pipes with Steel and synthetic fibers. *Construction and Building Materials*, Vol. 77, pp.218-226.

RILEM TC 162-TDF., 2002. Test and design methods for steel fibre reinforced concrete e bending test. *Material and Structures*, Vol. 36, pp.506-567.

Soylev T. and Ozturan T., 2014. Durability, physical and mechanical properties of fiber reinforced concretes at low fraction. *Construction and Building Materials*, pp.67-75.

UNE-EN 1916:2008. Concrete pipes and fittings, unreinforced, steel fibre and reinforced. 2008.